Scripta Materialia 247 (2024) 116086

Contents lists available at ScienceDirect

Scripta Materialia

journal homepage: www.journals.elsevier.com/scripta-materialia

On the athermal origin of flash sintering: Separating field-induced effects from Joule heating using a current ramp approach

Sandra Molina-Molina [a], Antonio Perejón [a,b,*], Luis A. Pérez-Maqueda [a], Pedro E. Sánchez-Jiménez [a,b,*]

[a] Instituto de Ciencia de Materiales de Sevilla, ICMSE CSIC-Universidad de Sevilla, C. Américo Vespucio 49, Sevilla, 41092, Spain
[b] Departamento de Química Inorgánica, Facultad de Química, Universidad de Sevilla, Sevilla, 41012, Spain

ARTICLE INFO

Keywords:
Flash sintering
Electric field
Joule heating
Current ramp
Zinc oxide

ABSTRACT

Joule heating is generally acknowledged as the main driving force behind Flash Sintering. However, this view is challenged by the presence of athermal phenomena and the similarities between the flash process and dielectric breakdown. This work offers new insights into flash as an electrical runaway. Using current ramps to perform flash experiments on zinc oxide, two distinct stages within the process were revealed by electrical, thermal and microstructural measurements: a field-dominated regime where the flash event is triggered and a subsequent current-dominated regime associated with power dissipation. The contribution of each regime to the whole flash process was found to be determined by the initial resistivity of the sample. Furthermore, impedance spectroscopy data confirmed field-induced enhancement of conductivity at the flash-onset without significant Joule heating.

First introduced in 2010 [1], Flash Sintering (FS) is already a well-established field-assisted sintering technique with a widening span of potential applications. When externally heated in the presence of an electric field, ceramic specimens undergo an abrupt increase in electrical conductivity. This so-called *flash event* leads to rapid densification at greatly reduced furnace temperatures for a broad variety of materials [2]. The origin of flash is generally accepted as a thermal runaway [3,4]. Still, certain phenomena cannot be explained merely in terms of Joule heating but rather as a consequence of the interaction between the material and the applied electric field. Frequency response of flashing systems under AC fields [5], electroluminescence [6], enhanced diffusion kinetics [7–9] and defect generation and migration [10,11] are some athermal effects detected during FS. In fact, it was hypothesized that a field-assisted mechanism of avalanche and nucleation of Frenkel defects, boosting diffusion rates and electrical conductivity, might be the cause of the flash event [12–14]. Similarly, field-driven defect generation in the oxide bulk is considered to be the physical mechanism accountable for dielectric breakdown in metal-oxide-semiconductor devices [15]. The many similarities between the flash phenomenon and dielectric breakdown continue to be explored [16,17] as evidence of discharge during FS has been found by ultraviolet corona effect detection [18] or phase-resolved partial discharge analysis [19].

Nevertheless, identifying these athermal, purely electrical features and separating their impact on FS from Joule heating is quite challenging due to the positive feedback loop existing between electrical current and temperature. Conventional FS (CFS) is performed under a constant field while the furnace temperature is either increased or kept constant. In both cases, the current freely rises up to a preset limit, causing uncontrolled heating of the sample. An alternative approach to improve thermal management during FS is the implementation of current ramps, which allows to reduce the heat generation rate by controlling the current traversing the specimen since the moment it starts to significantly flow [20]. The possibility of adjusting the ramp rate makes this methodology useful not only to avoid microstructural heterogeneity but also to tune porosity and grain size [21,22]. From a phenomenological perspective, Current Ramp FS (CRFS) also allows for a more detailed study of the flash process: the thermal profile and the length of the experiments can be regulated as desired.

In the present work, the joint evolution of temperature and electrical parameters during CRFS of Zinc oxide (ZnO) was analyzed in order to define the role of Joule heating and deconvolve it from field-assisted athermal effects. ZnO represents a suitable standard to investigate flash behavior since its sintering has been broadly studied both inside and outside FS literature [23–26]. Moreover, this material is highly sensitive to field effects because of its native arrangement of electrically active point defects, including zinc and oxygen vacancies, interstitials

* Corresponding authors.
E-mail addresses: aperejon@us.es (A. Perejón), pedro.enrique@icmse.csic.es (P.E. Sánchez-Jiménez).

https://doi.org/10.1016/j.scriptamat.2024.116086
Received 5 December 2023; Received in revised form 22 February 2024; Accepted 16 March 2024
Available online 26 March 2024

and antisites [27]. Around 0.8 g of a mixture of commercial powders of ZnO (Sigma-Aldrich, 544906 nanopowder, < 100 nm) and a 4% w/w polyvinyl alcohol (Sigma-Aldrich, 363162, 98.0 – 99 %) solution in distilled water were uniaxially pressed at 500 MPa into *dog-bone* samples with thickness of about 2 mm. The binder was removed by heating the pellets at 500 °C for 30 min, which were held inside a tubular furnace by two Ni-Cr wires connected to a DC power supply (EA-PSI 9750-06 DT). Platinum paste was applied to favor electrical contact between sample and electrodes. Electrical parameters were continuously recorded with a power analyzer (PPA1500 Newtons4th Ltd) and an infrared camera (PI 1 M, Optris GmbH) was used to register temperature data and to monitor the shrinkage of the samples. The CRFS experiments were performed at a constant furnace temperature of 700 °C. The power supply provided the required voltage for the current to follow a programmed linear ramp of 8 mAs^{-1} up to a current density limit of 100 $mAmm^{-2}$, which once reached was maintained for 1 min before turning the power supply and the furnace off. Three significant points were defined within a single experiment, as depicted in Fig. 1. The process was stopped at each one of these points, with the purpose of separately studying the evolution of the sample throughout the FS by means of electrical, thermal and microstructural measurements. A sample just heated up to 700 °C without applied field was microstructurally inspected as well. All samples were let to freely cool down to room temperature inside the furnace. Average grain sizes were estimated from SEM images by measuring the dimensions of 200 grains (Figure S1).

In CFS, after an incubation time dependent on temperature and field strength (usually known as Stage I), a sudden drop in electrical resistance signals the flash event and provokes a sharp rise of the current (Stage II) which is promptly restrained by the power supply to keep it constant (Stage III) [28]. Under CRFS conditions, the incubation time was shortened to less than 0.1 min, as the voltage was automatically increased until the sample became conductive enough to permit current flow. This was termed Point 1 or *flash-onset*, which essentially matches the Stage II observed in CFS. Basically, the material transitioned from insulator to conductor and consequently, the power supply switched from controlled-voltage (CV) to controlled-current (CC) mode. The field peaked at 110 Vcm^{-1} with a power density of 34 $mWmm^{-3}$ falling within the range usually required for triggering the flash event [29]. At that moment, the resistance of the material had dropped by more than 50% while the surface temperature of the sample was increased by roughly 30 °C (Fig. 1, right). No shrinkage was detected and SEM revealed a microstructure similar to the one found for the sample heated without applied field (Fig. 2a), with an estimated average grain size of (90 ± 30) nm. The specimen showed heterogeneous particle distribution and no signs of sintering or grain growth at Point 1 (Fig. 2b). Thus, the internal temperature reached at the flash-onset was not sufficient to cause visible microstructural changes. Joule heating was detected prior to the ramp but it was very limited due to the small associated current densities (3 $mAmm^{-2}$ at the beginning of the ramp). At the flash-onset, the emergence of conducting behavior on an initially insulating material was therefore not a consequence neither of densification nor Joule heating but presumably a field-induced phenomenon.

From the onset to the chosen limit of 100 $mAmm^{-2}$, the linear increase of current density was accompanied by power dissipation leading to the progressive heating and shrinkage of the sample throughout the whole ramp (Fig. 1, left). At the middle value of 50 $mAmm^{-2}$, named

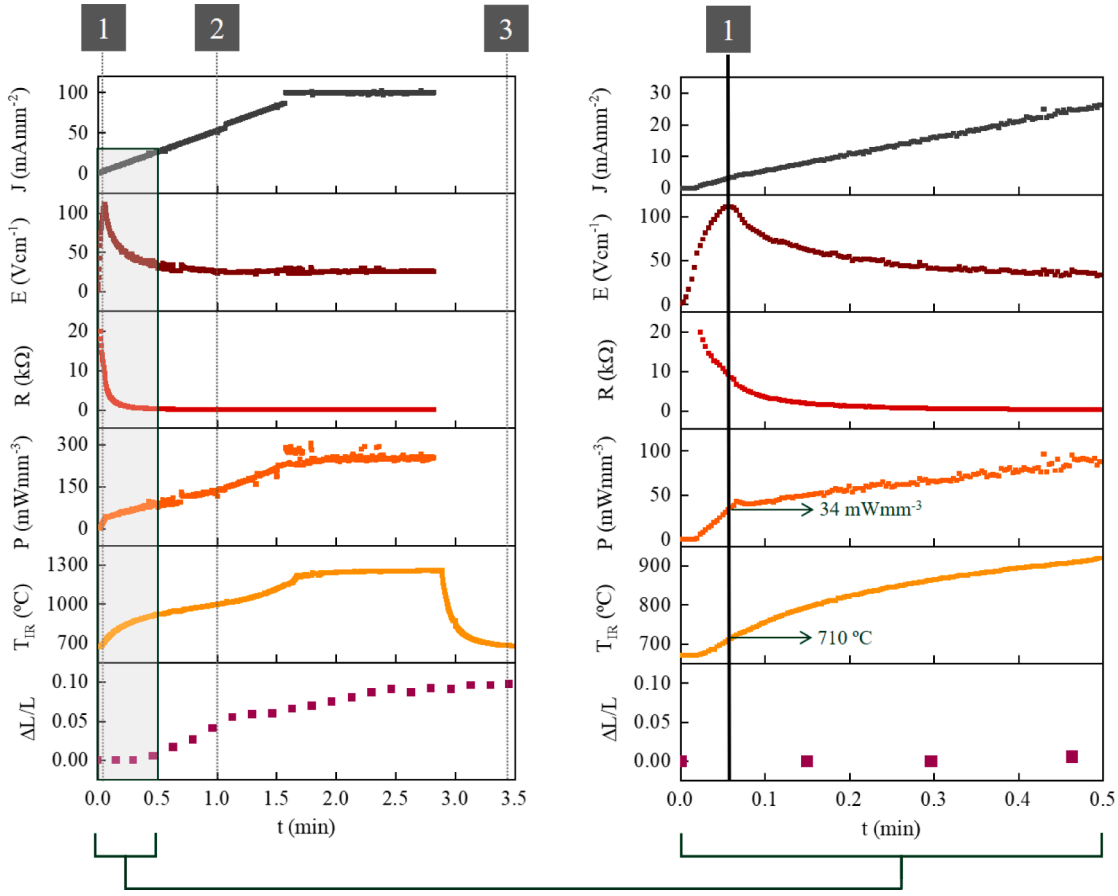

Fig. 1. Current density, electric field, resistance, power density, IR sample temperature and shrinkage evolution during CRFS of ZnO at a furnace temperature of 700 °C, current rate of 8 mAs^{-1}, current density limit of 100 $mAmm^{-2}$ and holding time of 1 min. Three points of interest were defined as Point 1 – flash-onset, Point 2 – interrupted ramp at its midpoint and Point 3 – complete ramp and cool-down. The plot on the right shows a magnified view of the region near the flash-onset as well as the electric power density and temperature values at Point 1.

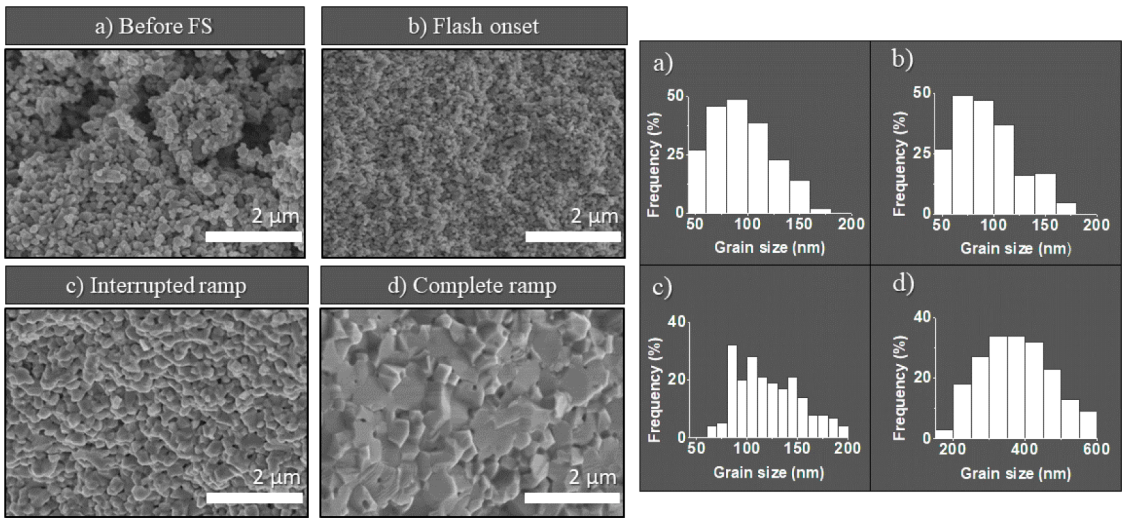

Fig. 2. SEM micrographs of cross-section fractures from the gauge length of the *dog-bone* (obtained using a Hitachi S-4800 FEG-SEM operated at 5 kV), and grain size distribution histograms of a) a ZnO sample heated at a furnace temperature of 700 °C without electric field and ZnO samples at b) Point 1 – flash-onset, c) Point 2 – interrupted ramp at its midpoint and d) Point 3 – complete ramp for CRFS at a furnace temperature of 700 °C, current rate of 8 mAs^{-1}, current density limit of 100 $mAmm^{-2}$ and holding time of 1 min.

Point 2, resistance had lowered by a 90% of its starting value and IR measurements estimated a surface temperature increase of ≈ 300 °C. Densification was ongoing at this point, as evidenced by the shrinkage profile and micrographs displaying enlarged grains with an average size of (120 ± 30) nm (Fig. 2c). Yet, sintering was not complete and space between grains was still discernible. Once the ramp was finished, Point 3 marked the end of the experiment after sustaining the current limit for 1 min with a total temperature increase of ≈ 600 °C. Reaching a final resistance of just 64 Ω, the specimen was almost fully dense after the complete FS process. A relative density of 97 % was obtained by the Archimedes' method taking 5.68 gcm^{-3} as theoretical density (JCPDS Ref. code 00-005-0664), which was consistent with SEM images showing a well-sintered material (Fig. 2d).

The linear control imposed over the current allowed the distinction between two different regimes of field and current within the same CRFS process. A first, field-dominated regime of high applied voltage causes a pronounced drop in resistance that ends up resulting in a current-dominated regime where resistance decreases gradually and densification concurs with Joule heating. These two regimes are present in CFS too, but the quickness of the uncontrolled current rise makes them look like one – simply known as Stage II. This separation between flash-onset and densification, with the latter heavily depending on the increase in temperature derived from power dissipation, has already been pointed out [30,31]. To address the athermal nature of the flash-onset, the focus could be put on how the electrical behavior of the material can be changed without significant power dissipation.

However, *ex-situ* characterization of the electrical properties of the specimen right after Point 1 is restricted by its low density. Impedance spectroscopy (IS) is a powerful technique to evaluate the electrical response of ceramics, but a dense specimen is required to obtain accurate results. Considering that any densification contribution to the conductivity can be dismissed in Point 1, as no sintering was observed, current ramp flash (CRF) experiments were conducted on dense ZnO *dog-bones*. In addition, the risk of preferential current path formation associated to microstructural heterogeneity can be minimized using dense samples. Previous densification was carried out at 1000 °C for 2 h in a box furnace with a heating and cooling rate of 10 °$Cmin^{-1}$. A furnace temperature of 700 °C and the same experimental conditions employed to flash-sinter ZnO green bodies were used to perform a CRF experiment with no holding time on a dense specimen (Figure S2). The starting resistivity of the sample was much lower because of its higher density so the field, resistance and temperature time profiles substantially differed from the CRFS ones. The flash-onset was no longer signaled by a field peak because of the current flowing from the very first moment the field was applied. In these conditions, the entwined evolution of current and field obstructs the study of any field-induced effects.

Thus, the insulator-to-conductor transition typical of FS could only be properly discriminated in dense ZnO samples if the starting insulating behavior was ensured by decreasing the furnace temperature. The different flash profiles recorded in experiments performed at furnace temperatures of 100 °C, 300 °C and 500 °C (Figure S3) showed that the initial resistivity is the key factor determining the balance between the field-dominated regime where the flash-onset takes place (higher resistance) and the following current-dominated regime (lower resistance) once the sample is conductive. According to those experiments, by decreasing the furnace temperature to 100 °C, the initial insulating behavior of the dense sample guaranteed a high applied field and sharp drop in electrical resistance.

To highlight the impact of the electric field, a series of CRF experiments were run at 100 °C up to different current density limits from 0.1 $mAmm^{-2}$ to 10 $mAmm^{-2}$. These low current values corresponded to the field-dominated regime of the flash process, well before the field peak (Figure S3a). By interrupting the experiment prior to the transition towards the current-dominated regime, Joule heating was minimized. Fig. 3 displays the applied field and temperature increase observed at the time the experiment is interrupted. The best compromise between the presence of a moderate field and no significant heating was found for 0.2 $mAmm^{-2}$. Below this value, the current limit was so small that it could be reached under a weak field without even triggering the flash. Above 0.2 $mAmm^{-2}$, the total sample temperature increment began to increase with the current density limit and the maximum field strength remained stable around 375 Vcm^{-1}, corresponding to the highest voltage the power supply could provide.

In order to preserve the defect structure of the material and prevent thermal defect annihilation, the sample subjected to a maximum current density of 0.2 $mAmm^{-2}$ was quenched by immersion in liquid nitrogen upon removal of the electric field, instead of being slowly cooled down inside the furnace. Afterwards, the electrical response of the specimen at room temperature was obtained by IS. The electrodes were fabricated from fast-drying silver paste on opposite faces of the gauge section of the *dog-bone*. For the sake of comparison, a dense ZnO sample heated up to

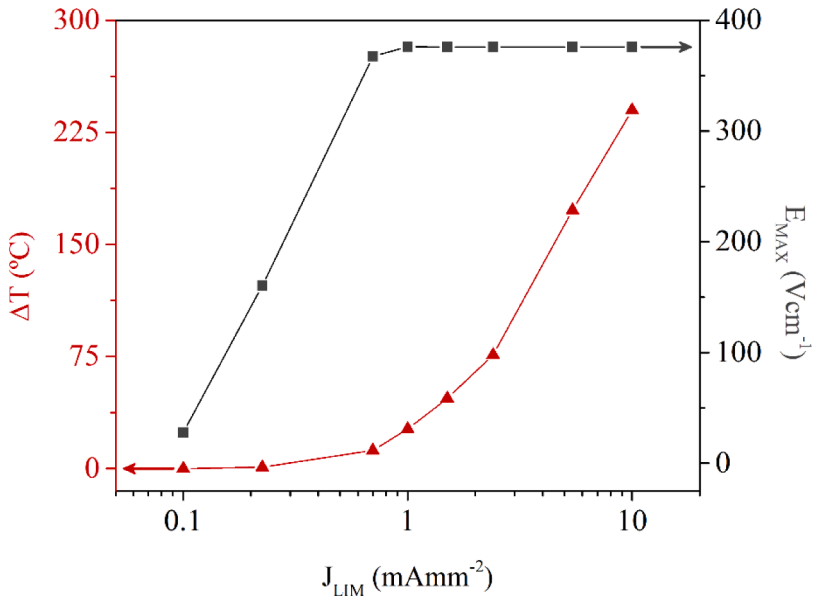

Fig. 3. Sample temperature increment (triangle) and maximum electric field strength (square) as a function of current density limit for a series of CRF experiments of dense ZnO at a furnace temperature of 100 °C.

100 °C without applied field and then quenched was also characterized. For both specimens, a semicircular feature appeared in the impedance complex plane representation (Fig. 4a). The arc was quite distorted in the case of the "no field" sample whereas the "field-applied" sample offered a more defined response along with lowered resistivity. This implies that the conductivity of dense ZnO was enhanced prior to the flash-onset. To reach the limit of 0.2 $mAmm^{-2}$ at a furnace temperature of 100 °C, a field peak of 178 Vcm^{-1} produced a resistance drop with negligible Joule heating (sample temperature increment of ≈ 1 °C as seen in Fig. 3).

To further study the nature of the increased conductivity, the "field-applied" sample was later heated at 350 °C for 3 h in air atmosphere according to previous works on thermal relaxation of ZnO defects [32,33]. IS confirmed the restoration of the resistivity of the sample after the annealing (Fig. 4a). Defect-related dielectric relaxation mechanisms were identified by examining the electric modulus spectra derived from the collected IS data. Fig. 4b shows the spectroscopic plots of the imaginary part of the electric modulus, M'', for the three studied samples. In the case of the "field-applied" sample, the displacement of the M'' peak towards higher frequencies indicates shorter relaxation times for the charge carriers [34,35]; on the other hand, the broadening of the M'' profile is the result of a wider distribution of relaxation times that can be ascribed to increased concentrations of different types of intrinsic defects [35]. The separation in the peak positions of the Z''/M'' spectra (Figure S4b) for the "field-applied" sample corresponds to a localized relaxation arising from short-range interactions in the bulk, consistent with previously reported intragranular defect formation in flash-sintered ZnO [36]. As opposed, long-range movement of charge carriers along grain boundaries is associated with Z''/M'' spectra overlapping [37], which can be observed for the "no field" sample (Figure S4a) and especially, for the "field-applied" sample after heating at 350 °C (Figure S4c).

Hence, the electric field modified the resistance distribution of the material (by defect migration, presumably) leading to increased conductivity. Following thermal relaxation of the altered defect structure, the initial resistivity and delocalized dielectric relaxation were restored. The finding of athermal resistance degradation is compatible with a dielectric breakdown mechanism. Both FS and breakdown are

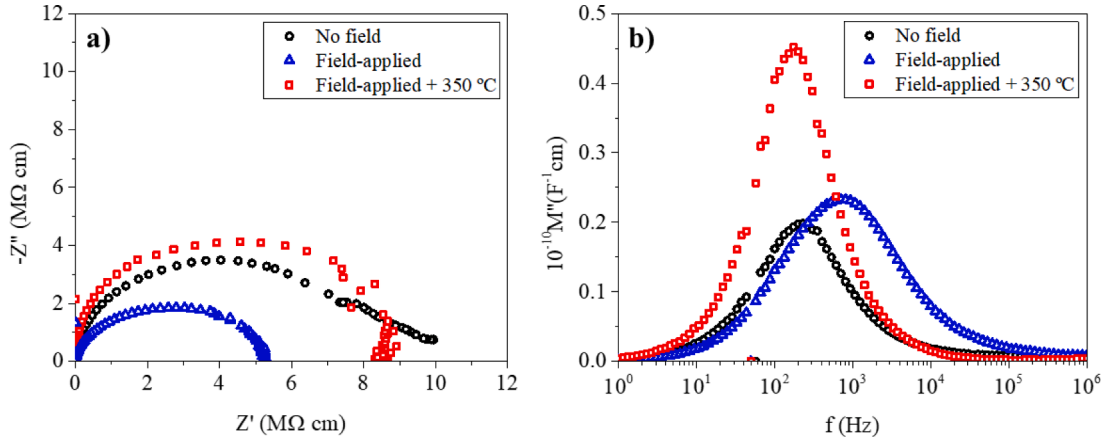

Fig. 4. a) Impedance complex plane plots and b) spectroscopic plots of the imaginary part of the electrical modulus at room temperature for samples of dense ZnO heated up to 100 °C and quenched by immersion in liquid nitrogen (no field, circle); heated up to 100 °C, subjected to a CRF experiment up to 0.2 $mAmm^{-2}$, then quenched (field-applied, triangle) and lastly, submitted to thermal treatment at 350 °C for 3 h in air atmosphere (field-applied + 350 °C, square). Measurements were performed with an AC measuring voltage of 0.1 V over a frequency range from 1 Hz to 1 MHz.

characterized by the transition from insulating to conducting behavior of a dielectric subjected to a sufficiently strong electric field. Though the fields involved in FS are commonly several orders of magnitude below the typical dielectric strength of ceramics (2–7 $kVcm^{-1}$ for ZnO [38]), it has been reported that this value can be reached by the amplification of the external field at the intergranular regions of the material [39]. Even if such a local field is not enough to directly trigger breakdown, a process of dielectric degradation known as *soft breakdown* or *time-dependent dielectric breakdown* can happen after a certain time [39], which is reminiscent of the FS incubation stage [40]. Breakdown finally occurs when a conductive percolation path of defects generated under field stress forms across the electrodes [15].

Enhancement of electrical conductivity in flash-sintered materials is habitually attributed to their microstructures being finer than those of their conventionally prepared analogues [41,42]. But previous works have found increased *ex-situ* grain boundary conductivity for flashed 8-mol% Yttria-stabilized zirconia not explainable by thermal history [30] and also defect formation leading to a considerable increase in conductivity after FS of ZnO [36]. This study further shows that the application of a modest electric field suffices to alter the electrical properties of ZnO, triggering the conducting behavior that leads to current flow and power dissipation in the later stages of flash processes.

Thus, the flash-onset should be considered the cause of Joule heating and not a consequence, at least under the studied conditions. For conventional FS and very conductive samples instead, the process is mostly current-dominated because of a smoother resistance decrease related to gradual power dissipation and eventually, thermal runaway. Future work shall include looking for direct evidence of breakdown in these cases and also under the influence of moderate fields, since the majority of works reporting discharge focus on FS under strong electric fields in the order of $kVcm^{-1}$ [43]. In any case, FS might be regarded as an electrical runaway rather than a thermal runaway: the parameter that ultimately determines if the process is dominated by the field or by Joule heating is the starting electrical resistivity of the material.

Declaration of competing interest

The authors declare that they have no known competing financial interests or personal relationships that could have appeared to influence the work reported in this paper.

Acknowledgements

This work was supported by Junta de Andalucía-Consejería de Conocimiento, Investigación y Universidad project P18-FR-1087 (Junta de Andalucía-Consejería de Conocimiento, Investigación y Universidad – Fondo Europeo de Desarrollo Regional (FEDER), Programa Operativo FEDER Andalucía 2014–2020) and INTRAMURAL-CSIC grant numbers 201960E092 and 202060I004.

Supplementary materials

Supplementary material associated with this article can be found, in the online version, at doi:10.1016/j.scriptamat.2024.116086.

References

[1] M. Cologna, B. Rashkova, R. Raj, Flash Sintering of Nanograin Zirconia in <5 s at 850°C, J. Am. Ceram. Soc. 93 (11) (2010) 3556–3559.
[2] M. Yu, S. Grasso, R. McKinnon, T. Saunders, M.J. Reece, Review of flash sintering: materials, mechanisms and modelling, Adv. Appl. Ceram. 116 (1) (2016) 24–60.
[3] R.I. Todd, E. Zapata-Solvas, R.S. Bonilla, T. Sneddon, P.R. Wilshaw, Electrical characteristics of flash sintering: thermal runaway of Joule heating, J. Eur. Ceram. Soc. 35 (6) (2015) 1865–1877.
[4] Y. Zhang, J.-I. Jung, J. Luo, Thermal runaway, flash sintering and asymmetrical microstructural development of ZnO and ZnO–Bi2O3 under direct currents, Acta Mater. 94 (2015) 87–100.
[5] S. Molina-Molina, A. Perejón, L.A. Pérez-Maqueda, P.E. Sánchez-Jiménez, Influence of AC Fields and Electrical Conduction Mechanisms On the Flash-Onset temperature: Electronic (BiFeO3) vs. Ionic Conductors (8YSZ), Ceramics International, 2022.
[6] D. Yadav, R. Raj, Two unique measurements related to flash experiments with yttria-stabilized zirconia, J. Am. Ceram. Soc. 100 (12) (2017) 5374–5378.
[7] J. Narayan, A new mechanism for field-assisted processing and flash sintering of materials, Scr. Mater. 69 (2) (2013) 107–111.
[8] Y. Sasaki, K. Morita, T. Yamamoto, K. Soga, H. Masuda, H. Yoshida, Electric current dependence of plastic flow behavior with large tensile elongation in tetragonal zirconia polycrystal under a DC field, Scr. Mater. (2021) 194.
[9] K. Morita, F. Naito, D. Terada, Microcrack healing in zirconia ceramics under a DC electric field/current, J. Eur. Ceram. Soc. 41 (16) (2021) 282–289.
[10] O. Guillon, R.A. De Souza, T.P. Mishra, W. Rheinheimer, Electric-field-assisted processing of ceramics: nonthermal effects and related mechanisms, MRS Bulletin 46 (1) (2021) 52–58.
[11] R. Raj, Joule heating during flash-sintering, J. Eur. Ceram. Soc. 32 (10) (2012) 2293–2301.
[12] K.S. Naik, V.M. Sglavo, R. Raj, Flash sintering as a nucleation phenomenon and a model thereof, J. Eur. Ceram. Soc. 34 (15) (2014) 4063–4067.
[13] M. Jongmanns, R. Raj, D.E. Wolf, Generation of Frenkel defects above the Debye temperature by proliferation of phonons near the Brillouin zone edge, New. J. Phys. 20 (9) (2018).
[14] M. Jongmanns, D.E. Wolf, Element-specific displacements in defect-enriched TiO2: indication of a flash sintering mechanism, J. Am. Ceram. Soc. 103 (1) (2019) 589–596.
[15] S. Lombardo, J.H. Stathis, B.P. Linder, K.L. Pey, F. Palumbo, C.H. Tung, Dielectric breakdown mechanisms in gate oxides, J. Appl. Phys. 98 (12) (2005).
[16] M. Biesuz, P. Luchi, A. Quaranta, V.M. Sglavo, Theoretical and phenomenological analogies between flash sintering and dielectric breakdown in α-alumina, J. Appl. Phys. 120 (14) (2016) 145107.
[17] R. Shi, Y. Pu, J. Ji, J. Li, X. Guo, W. Wang, M. Yang, Correlation between flash sintering and dielectric breakdown behavior in donor-doped barium titanate ceramics, Ceram. Int. 46 (8) (2020) 12846–12851.
[18] J. Liu, H. Rongxia, R. Zhang, G. Liu, X. Wang, Z. Jia, L. Wang, Mechanism of flash sintering with high electric field: in the view of electric discharge and breakdown, Scr. Mater. 187 (2020) 93–96.
[19] J.F. Fagnard, C. Gajdowski, L. Boilet, F. Henrotte, C. Geuzaine, B. Vertruyen, P. Vanderbemden, Use of partial discharge patterns to assess the quality of sample/electrode contacts in flash sintering, J. Eur. Ceram. Soc. 41 (1) (2021) 669–683.
[20] M.K. Kumar, P.D. Yadav, J.M. Lebrun, R. Raj, Flash sintering with current rate: a different approach, J. Am. Ceram. Soc. 102 (2) (2019) 823–835.
[21] H. Charalambous, S.K. Jha, K.H. Christian, R.T. Lay, T. Tsakalakos, Flash Sintering using Controlled Current Ramp, J. Eur. Ceram. Soc. 38 (10) (2018) 3689–3693.
[22] R. Lavagnini, I.J.V. Campos, J.A. Ferreira, E.M.J.A. Pallone, Microstructural evolution of 3YSZ flash-sintered with current ramp control, J. Am. Ceram. Soc. 103 (6) (2020) 3493–3499.
[23] T.K. Roy, D. Bhowmick, D. Sanyal, A. Chakrabarti, Sintering studies of nano-crystalline zinc oxide, Ceram. Int. 34 (1) (2008) 81–87.
[24] C. Schmerbauch, J. Gonzalez-Julian, R. Röder, C. Ronning, O. Guillon, L. Gauckler, Flash Sintering of Nanocrystalline Zinc Oxide and its Influence on Microstructure and Defect Formation, J. Am. Ceram. Soc. 97 (6) (2014) 1728–1735.
[25] X.L. Phuah, H. Wang, H. Charalambous, S.K. Jha, T. Tsakalakos, X. Zhang, H. Wang, Comparison of the grain growth behavior and defect structures of flash sintered ZnO with and without controlled current ramp, Scr. Mater. 162 (2019) 251–255.
[26] Y. Zhang, J. Nie, J.M. Chan, J. Luo, Probing the densification mechanisms during flash sintering of ZnO, Acta Mater. 125 (2017) 465–475.
[27] M.D. McCluskey, S.J. Jokela, Defects in ZnO, J. Appl. Phys. 106 (7) (2009).
[28] S.K. Jha, K. Terauds, J.-M. Lebrun, R. Raj, Beyond flash sintering in 3 mol% yttria stabilized zirconia, Journal of the Ceramic Society of Japan 124 (4) (2016) 283–288.
[29] R. Raj, Analysis of the Power Density at the Onset of Flash Sintering, J. Am. Ceram. Soc. 99 (10) (2016) 3226–3232.
[30] C.A. Grimley, S. Funni, C. Green, E.C. Dickey, A thermal perspective of flash sintering: the effect of AC current ramp rate on microstructure evolution, J. Eur. Ceram. Soc. 41 (4) (2021) 2807–2817.
[31] S. Bhandari, T.P. Mishra, O. Guillon, D. Yadav, M. Bram, Accessing the role of Joule heating on densification during flash sintering of YSZ, Scr. Mater. 211 (2022) 114508.
[32] H. Zeng, X. Ning, X. Li, An insight into defect relaxation in metastable ZnO reflected by a unique luminescence and Raman evolutions, Physical Chemistry Chemical Physics 17 (29) (2015) 19637–19642.
[33] W.C. Lim, J.P. Singh, Y. Kim, J. Song, K.H. Chae, T.-Y. Seong, Effect of thermal annealing on the properties of ZnO thin films, Vacuum. 183 (2021) 109776.
[34] A.K. Bhunia, S.S. Pradhan, K. Bhunia, A.K. Pradhan, S. Saha, Study of the optical properties and frequency-dependent electrical modulus spectrum to the analysis of electric relaxation and conductivity effect in zinc oxide nanoparticles, Journal of Materials Science: Materials in Electronics 32 (17) (2021) 22561–22578.
[35] Z. Fu, J. He, J. Lu, Z. Fang, B. Wang, Investigation of dielectric relaxation and degradation behavior of two-step sintered ZnO varistors, Ceram. Int. 45 (17, Part A) (2019) 21900–21909.
[36] H. Gao, T.J. Asel, J.W. Cox, Y. Zhang, J. Luo, L.J. Brillson, Native point defect formation in flash sintered ZnO studied by depth-resolved cathodoluminescence spectroscopy, J. Appl. Phys. 120 (10) (2016) 105302.

[37] M. Coşkun, Ö. Polat, F.M. Coşkun, Z. Durmuş, M. Çağlar, A. Türüt, The electrical modulus and other dielectric properties by the impedance spectroscopy of $LaCrO_3$ and $LaCr_{0.90}Ir_{0.10}O_3$ perovskites, RSC. Adv. 8 (9) (2018) 4634–4648.
[38] L. Meng, L. Zheng, L. Cheng, G. Li, L. Huang, Y. Gu, F. Zhang, Synthesis of novel core-shell nanocomposites for fabricating high breakdown voltage ZnO varistors, J. Mater. Chem. 21 (30) (2011) 11418.
[39] T.B. Holland, U. Anselmi-Tamburini, D.V. Quach, T.B. Tran, A.K. Mukherjee, Local field strengths during early stage field assisted sintering (FAST) of dielectric materials, J. Eur. Ceram. Soc. 32 (14) (2012) 3659–3666.
[40] K.S.N. Vikrant, H. Wang, A. Jana, H. Wang, R.E. García, Flash sintering incubation kinetics, NPJ. Comput. Mater. 6 (1) (2020).
[41] R. Muccillo, E.N.S. Muccillo, An experimental setup for shrinkage evaluation during electric field-assisted flash sintering: application to yttria-stabilized zirconia, J. Eur. Ceram. Soc. 33 (3) (2013) 515–520.
[42] J.C. M'Peko, J.S.C. Francis, R. Raj, Impedance Spectroscopy and Dielectric Properties of Flash Versus Conventionally Sintered Yttria-Doped Zirconia Electroceramics Viewed at the Microstructural Level, J. Am. Ceram. Soc. 96 (12) (2013) 3760–3767.
[43] H. Zhou, X. Li, Y. Zhu, J. Liu, A. Wu, G. Ma, X. Wang, Z. Jia, L. Wang, Review of flash sintering with strong electric field, High Voltage 7 (1) (2022) 1–11.